ÓPTICA PURA Y APLICADA
www.sedoptica.es

Type: RIAO OPTILAS 2023
Section: IMAGING TECHNIQUES

Impact of image resolution on retinal vessel tortuosity assessment

Efecto de la resolución de la imagen en la evaluación de la tortuosidad de los vasos retinales

N. Ramírez *, M. Ralló, M.S. Millan[S]
Grupo de Óptica Aplicada y Procesado de Imagen, Universitat Politècnica de Catalunya-BarcelonaTECH

(*) E-mail: natalia.ramirezcano@gmail.com, m.millan@upc.edu S: miembro de SEDOPTICA / SEDOPTICA member

Received: 21/12/2023 Accepted: 06/02/2024
DOI: 10.7149/OPA.57.1.51171

ABSTRACT: Several ocular and cardiovascular disorders are characterized by an elevated tortuosity of retinal blood vessels. Objective tortuosity measurements can be obtained through the computation of a set of tortuosity indices derived from digital image analysis of an eye fundus image. These calculations require the parametrization of the vessel path traced in the image. As a vessel descriptor, tortuosity should be independent of scale, but this property demands thorough examination and assessment for each index. We investigate the impact of altering image resolution on the local tortuosity indices of retinal vessels.

Key words: retinal vessels, tortuosity, image resolution, image scaling, curvature.

RESUMEN: Algunas enfermedades oculares y cardiovasculares presentan un aumento de la tortuosidad de los vasos sanguíneos de la retina. Se pueden obtener medidas objetivas de la tortuosidad a través del cálculo de un conjunto de índices de tortuosidad mediante análisis digital imágenes del fondo de ojo (o retinografías). Este cálculo requiere la parametrización de la curva dibujada por el vaso en la imagen. Los descriptores de los vasos deben ser independientes de la escala (resolución) de la imagen, pero esta propiedad debe ser estudiada y evaluada para cada índice de tortuosidad. Nosotros analizamos cómo un cambio en la resolución de la imagen de fondo de ojo afecta a los índices de tortuosidad locales de los vasos retinianos.

Palabras clave: vasos retinales, tortuosidad, resolución de la imagen, escalado de imagen, curvatura.

REFERENCES AND LINKS / REFERENCIAS Y ENLACES

[1] M. A. Vilela, C. E. Amaral, M. A. T Ferreira, “Retinal vascular tortuosity: Mechanisms and measurements,” Eur J Ophthalmol **31**, 1497-1506 (2021).

[2] W. E. Hart, M. Goldbaum, B. Côté, P. Kube, M. R. Nelson, “Measurement and classification of retinal vascular tortuosity,” Int J Med Inform **53**, 239-252 (1999).

[3] A. A. Kalitzeos, G. Y. H. Lip, R. Heitmar, “Retinal vessel tortuosity measures and their applications,” Exp Eye Res **106**, 40-66 (2013).

[4] E. Grisan, M. Foracchia, A. Ruggeri, “A novel method for the automatic grading of retinal vessel tortuosity,” IEEE Trans Med Imaging **27**, 310-319 (2008).

[5] N. Ramírez, M. Ralló, M. S. Millan, "Retinal Vessel Local Tortuosity under a Macula-to-Optic Disc Central-Framing Change," Diagnostics **13**, 1030 (2023).

[6] O. Smedby, N. Högman, S. Nilsson, U. Erikson, A. G. Olsson, G. Walldius, “Two-dimensional tortuosity of the superficial femoral artery in early atherosclerosis,” J Vasc Res **30**, 181-191 (1993).

[7] R. Bernardes, P. Serranho, C. Lobo, “Digital ocular fundus imaging: a review,” Ophthalmologica **226**, 161-181 (2011).

[8] R. Turior, D. Onkaew, B. Uyyanonvara. "PCA-based retinal vessel tortuosity quantification," IEICE transactions on information and systems **96**, 329-339 (2013).

[9] T. Lewiner, J. Gomes, D. Lopes, M. Craizer, "Curvature and torsion estimators based on parametric curve fitting," Computers & Graphics **29**, 641-655 (2005).

1. Introduction

An increased tortuosity of the retinal vessels is a biomarker of severity, longevity, prognosis, and therapeutic response in countless clinical situations [1]. Its relevance results from the possibility to observe it noninvasively in eye's fundus digital images.

There are many indices available to assess tortuosity of retinal vessels [2,3], providing local tortuosity measures for any vessel segment extracted from a retinal vessel tree. Most tortuosity indices are calculated from a parametrization of the curve describing the centerline of the vessel segment under analysis. Their definitions rely on geometric features of that curve: chord, length and curvature [2-4]. To make these geometric features, and thus the local tortuosity values, independent from the parametrization used to describe that curve, we interpret their definitions as line integrals with respect to arc length [5], in accordance with the original definitions of Smedby et al. [6].

The selection of an appropriate tortuosity index should be guided by its performance characteristics. In our previous work [5], we investigated the impact of digital fundus image centering (either at the optic disc or macula) on tortuosity measurements. In this study, we extend our analysis to examine the effect of image resolution on tortuosity indices.

The inherent geometric formulation of tortuosity indices [2-5] renders them independent of vessel segment location, unaffected by translation or rotation. However, certain indices remain susceptible to scale variations. Specifically, a reduced-scale representation of a vessel segment will result in a shorter length, shorter chord, and higher curvature. Hart et al. [2] theoretically examined the impact of scale alterations on local tortuosity measures in the continuous setting.

Digital eye fundus images exhibit a wide range of resolutions in pixels, primarily due to the diverse sensor resolutions of fundus cameras, storage capacity limitations, and varying field scopes [7]. When analyzing lines segmented from digital images, it is common to adopt the pixel size as the unit of length. Consequently, resolution in the discrete (digital) setting plays an analogous role to scale in the continuous setting. Therefore, understanding the effect of resolution on tortuosity values is crucial for comparing the results of research studies involving tortuosity analysis based on fundus images of varying sizes. Turior et al. [8] evaluated two of the tortuosity indices considered by Hart, distance factor and total curvature, for the same sinusoidal curve presented at three different resolutions and found no resolution effects. Turior et al. asserted that "any useful tortuosity index should be independent of scale".

In this work, we analyze rescaled versions of simulated and actual digital images of retinal vessel segments to investigate the effect of resolution on the tortuosity values obtained from eight different indices based on geometric features. This analysis provides insights into the performance of these indices, enabling their informed selection and facilitating the comparison of research works regardless of the pixel size of digital fundus images.

2. Background: local tortuosity indices. Scaling effect in the continuous setting.

Let us consider the tortuosity indices analyzed by Hart et al. [2] and Kalitzeos et al. [3]. The centerline of a vessel segment (Fig. 1) can be described by a parameterized curve $C = \big(x(t), y(t)\big)$ with $t_0 \le t \le t_1$. The parameter values t_0 and t_1 correspond to the initial and final endpoints, respectively. The curvature is given by

$$\kappa(t) = \frac{y''(t) \cdot x'(t) - y'(t) \cdot x''(t)}{(x'(t)^2 + y'(t)^2)^{\frac{3}{2}}} \qquad (1)$$

whose units are usually expressed in radians per unit of length. In Eq.1, $\big(x'(t), y'(t)\big)$ and $\big(x''(t), y''(t)\big)$ denote the first and second derivatives of $\big(x(t), y(t)\big)$, respectively. The tortuosity indices are formulated in terms of several geometric features of this parametric curve: distance between endpoints or chord (D), curve length (L), total curvature (TK), and total squared curvature (TSK), as presented in Table 1 with their

corresponding units. To be more precise, TK represents the total absolute curvature because it uses the absolute value of the curvature instead of the signed curvature. We presume that the values of these geometric features should be independent of the parametrization used to represent the curve. Consequently, we interpret the definitions of the geometric features provided by Hart [2] as integrals with respect to arc length, which aligns more closely with the original definitions proposed by Smedby et al. [6].

TABLE 1. Geometric features involved in the definitions of the tortuosity indices (Table 2).

Chord	$D = \sqrt{(x(t_1) - x(t_0))^2 + (y(t_1) - y(t_0))^2}$	unit of length	(2)
Curve length	$L = \int_C 1\, ds = \int_{t_0}^{t_1} 1 \cdot \sqrt{x'(t)^2 + y'(t)^2}\, dt$	unit of length	(3)
Total curvature	$TK = \int_C \lvert\kappa\rvert\, ds = \int_{t_0}^{t_1} \lvert\kappa(t)\rvert \cdot \sqrt{x'(t)^2 + y'(t)^2}\, dt$	radians	(4)
Total squared curvature	$TSK = \int_C \kappa^2\, ds = \int_{t_0}^{t_1} \kappa^2(t) \cdot \sqrt{x'(t)^2 + y'(t)^2}\, dt$	radians²/unit of length	(5)

Table 2 contains the definitions of the eight tortuosity indices analyzed in this study. These indices are formulated in terms of the geometric features listed in Table 1.

TABLE 2. Definitions of the tortuosity indices (DF, T1 ...T7) in terms of the geometric features listed in Table 1.

Tortuosity index	DF	$T1$	$T2$	$T3$	$T4$	$T5$	$T6$	$T7$
Expression	$\frac{L}{D}$	$\frac{L}{D} - 1$	TK	TSK	$\frac{TK}{L}$	$\frac{TSK}{L}$	$\frac{TK}{D}$	$\frac{TSK}{D}$

Figure 1 illustrates the concept behind the simplest tortuosity index, the distance factor (DF): the ratio of the vessel segment centerline length (L) to the chord length connecting its endpoints (D). DF equals 1 for a straight-line segment between these endpoints, whereas DF exceeds 1 for any curved path with the same endpoints. The greater the sinuosity of the path, the higher the value of the DF index.

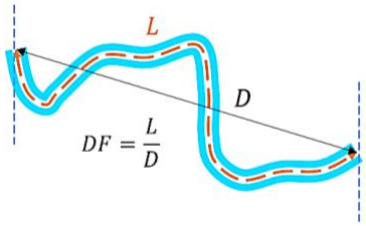

Fig.1. DF index as the ratio of length (L) and chord (D).

A scale change of factor $\boldsymbol{\alpha > 0}$ in the continuous setting transforms the curve $\boldsymbol{C = (x(t), y(t))}$ with $\boldsymbol{t_0 \le t \le t_1}$ into its scaled version $\boldsymbol{C_\alpha = (x_\alpha(t), y_\alpha(t)) = (\alpha \cdot x(t), \alpha \cdot y(t))}$ with $\boldsymbol{t_0 \le t \le t_1}$. The scaling effects on the geometric features can be calculated from their mathematical definitions (Table 3). See, for instance, the effect of a scale change $\boldsymbol{\alpha}$ on the curvature function (Eq.1):

$$\kappa_\alpha(t) = \frac{y''_\alpha(t) \cdot x'_\alpha(t) - y'_\alpha(t) \cdot x''_\alpha(t)}{(x'^2_\alpha(t) + y'^2_\alpha(t))^{\frac{3}{2}}} = \frac{\alpha \cdot y''(t) \cdot \alpha \cdot x'(t) - \alpha \cdot y'(t) \cdot \alpha \cdot x''(t)}{((\alpha \cdot x'(t))^2 + (\alpha \cdot y'(t))^2)^{\frac{3}{2}}} = \frac{1}{\alpha}\kappa(t)\,,$$

where κ_α stands for the curvature of C_α.

TABLE 3. Scaling effects on the geometric features of the parameterized curve C. C_α is a scaled version of C with scale factor α.

	C	C_α
Chord	D	$\alpha \cdot D$
Curve length	L	$\alpha \cdot L$
Total curvature	TK	TK
Total squared curvature	TSK	TSK/α

The scaling effects of the α factor on the values of the tortuosity indices (Table 4) can be straightforwardly computed from Tables 2 and 3. It is noteworthy that *DF*, *T1*, and *T2* are the only indices that remain scale-independent when considering curves in the continuous setting, consistent with the findings reported by Turior et al. [8].

TABLE 4. Scaling effects on the tortuosity indices of the parameterized curve C. C_α is a scaled version of C with scale factor α.

Index for C	DF	$T1$	$T2$	$T3$	$T4$	$T5$	$T6$	$T7$
Index for C_α	DF	$T1$	$T2$	$\frac{T3}{\alpha}$	$\frac{T4}{\alpha}$	$\frac{T5}{\alpha^2}$	$\frac{T6}{\alpha}$	$\frac{T7}{\alpha^2}$

3. Vessel segment simulations and scaling effects.

Digital image scaling, which is related to sampling frequency, produces digital images with varying pixel dimensions. The term 'image resolution' is commonly used to refer to these sizes. To evaluate the impact of image resolution on tortuosity index values, we simulated vessel segments using curves defined by known mathematical formulas (sinusoids), allowing for the precise calculation of tortuosity. This approach is not applicable to actual vessel segments, as their centerlines lack exact mathematical formulations. Therefore, we additionally present an alternative method for extracting tortuosity values from digital curve images.

3.a Continuous and discrete simulations of a vessel segment.

We have already seen the scaling effects on the tortuosity indices in a continuous setting (Table 4). Let us draw our attention to the effects in a discrete setting. While the original continuous curve $C = (x(t), y(t))$ with $t_0 \leq t \leq t_1$ can be exactly reconstructed from a lower-scaled version, $C_\alpha = (x_\alpha(t), y_\alpha(t)) = (\alpha \cdot x(t), \alpha \cdot y(t))$ with $t_0 \leq t \leq t_1$ and $0 < \alpha < 1$, by simply rescaling it by α^{-1}, this is not possible for discrete curves, particularly those derived from digital images. A low-resolution version of a discrete curve lacks the necessary information to precisely recover the original one. Information loss is associated with resolution reduction and may also depend on the curve's shape, with highly tortuous curves potentially experiencing greater loss. This information loss could impact tortuosity assessment.

To emulate the scenario of eye fundus imaging and retinal vessel tortuosity assessment from digital images, we employ a sinusoidal curve to simulate the centerline of a vessel segment. By varying the frequency ω, we replicate the sinusoid with different degrees of tortuosity (a digital version is displayed on Fig. 2). We consider $A \times A$ square images with pixel sizes of $A = \{100, 200, 400, 800\}$ to represent the range from critical to common resolutions for digital eye fundus images. For simplicity, the curve plots appear in white against a black background, centered within the image, and span over $3/5$ of the horizontal dimension and $2/3$ of the vertical dimension.

For each A and ω, a continuous sine curve was exactly parametrized according to the expression

$$C = (x(t), y(t)) = \left(\frac{A}{5} + \frac{3At}{5}, \frac{A}{2} + \frac{A}{3}\sin(2\pi\omega t)\right), \quad \text{with } 0 \leq t \leq 1, \qquad (6)$$
$$A = 100, 200, 400, 800; \qquad \omega = 1.0, 1.5, 2.0, 2.5,$$

being ω the frequency of the sinusoid and A the pixel dimension of the simulated image. For each A, the sinusoidal curve spans $\frac{3A}{5}$ of the image's horizontal dimension, leaving a black margin of $\frac{A}{5}$ on either side. For a given ω value, there are four scaled versions of the sinusoidal curve.

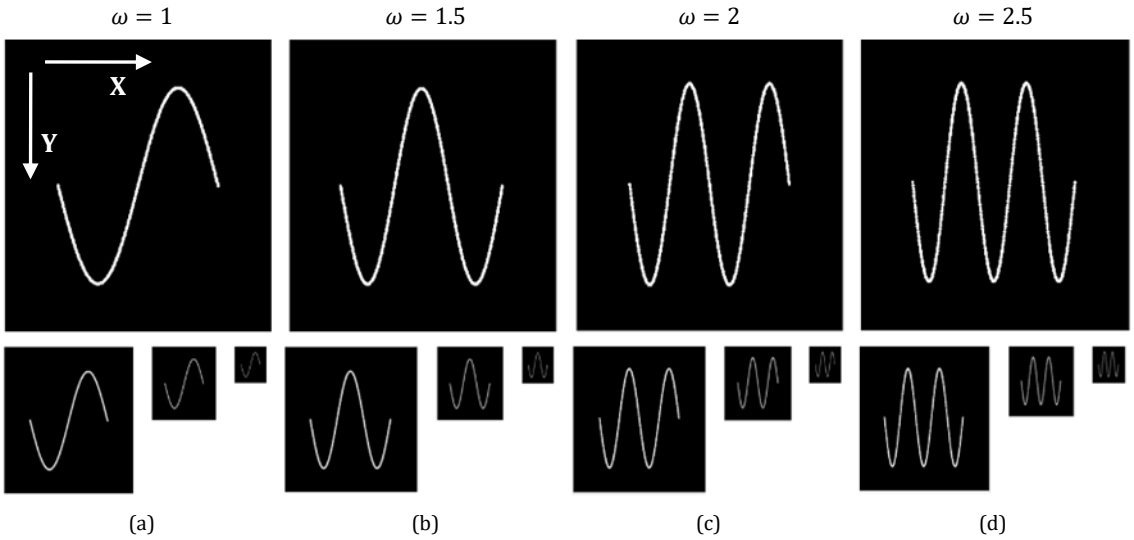

Fig 2. Sinusoids and scaled versions. X and Y indicate the positive axes. ω represents the frequency.

For $\omega = 1$ and $A = 800$, we generated a binary image 800×800 pixel size (top sinusoid in Fig. 2(a)) by assigning the value 1 to the pixel in column $x\left(\frac{k}{480}\right)$ and row round$(y\left(\frac{k}{480}\right))$, with $k = 0,1, \dots, \frac{3A}{5} = 480$, and the value 0 to the rest of pixels. We subsequently filled in the possible blank spaces existing between consecutive pixels of the sine curve by linear interpolation to obtain a connected curve (8-connectivity). We proceeded analogously with the rest of frequencies.

To generate lower-resolution versions (400×400, 200×200, and 100×100) from the initial 800×800 images, we followed this three-step procedure:

1. Applying a slight morphological dilation with a circular structuring element of size 5 to the initial sinusoidal curve.
2. Reducing the image dimension by half using bicubic interpolation.
3. Performing skeletonization.

This procedure is consistent with the one applied later to obtain lower-resolution versions of the centerlines of actual vessel segments extracted from real digital fundus images.

Discrete parametrization $C_s = (x_s, y_s)$ of those digital simulations resulted straightforwardly by sampling the continuous parametrization (Eq. 6) of the sinusoids

$$C_s = \left(x_s(k), y_s(k)\right) = \left(\frac{A}{5} + \frac{3Ak}{5N_s}, \frac{A}{2} + \frac{A}{3}\sin\left(2\pi\omega\frac{k}{N_s}\right)\right), \quad \text{with } k = 0,1, \dots, N_s\,, \qquad (7)$$
$$A = 100, 200, 400, 800;\ \omega = 1.0, 1.5, 2.0, 2.5,$$

where N_s is the total number of pixels of the connected sinusoidal plot.

Such discrete parametrizations are not achievable from digital images of actual segmented vessel segments, whose centerline lacks any exact mathematical expression. For this reason, we alternatively considered another parametrization of the curve obtained from the digital image alone, as we reported in a previous work [5]. We applied it here to a sinusoidal segment. We counted its number of pixels (N_s) and found the pixel of the sinusoidal segment with coordinates closest to the position $\left(1, \frac{A}{2}\right)$ (left end of the horizontal central line). This pixel was labeled the first point of the string. The algorithm iteratively identified the next closest pixel among the remaining pixels. This process continued until all pixels had been assigned to the string. A final smoothing operation with a 3-term moving average of both x and y strings provided the parametrization $C_i = \left(x_i(k), y_i(k)\right)$, $k = 1,2, \dots N_s$ of the complete sinusoid segment based exclusively on the plot image. The parametrization obtained this way from each image and its resized versions are ready to be used for the discrete computation of tortuosity indices.

The continuous exact parametrization $C = \left(x(t), y(t)\right)$ (Eq. 6) allowed us to obtain the exact values of the tortuosity indices for the various sinusoids and their scaled continuous versions. The discrete parametrizations $C_s = \left(x_s(t), y_s(t)\right)$ (Eq. 7) obtained by direct sampling and those obtained from the

sinusoids plot images $C_i = (x_i(t), y_i(t))$ led us to obtain other sets of values of the tortuosity indices affected by scaling and discretization. The results and comparisons are presented in the next section.

3.b Scaling effects for the simulated segments.

Table 5 presents the values of the exact calculation of the geometric features for the sinusoids in various scales as illustrated in Fig. 2. These values were calculated using the formulas in Table 1 and the continuous parametrizations provided in Equation 6. Numerical integration methods were employed when necessary. Note that chord and curve length values exhibit a linear increase with increasing image resolution. Observe the independence of total curvature from image resolution and the linear decrease total squared curvature as image resolution increases. Additionally, note the influence of increasing frequency on the curve length, total curvature, and total squared curvature, which all increase accordingly. However, chord values remain unaffected by varying frequency, as it can be expected from its definition (Fig. 1 and Eq.2).

TABLE 5. Exact calculation of the geometric features of the sinusoids (Fig. 2) for various image sizes (A) and frequencies (ω).

Geometric feature	Frequency	Resolution (image size)			
	ω	$A = 100$	$A = 200$	$A = 400$	$A = 800$
Chord (D)	1.0	60	120	240	480
	1.5	60	120	240	480
	2.0	60	120	240	480
	2.5	60	120	240	480
Curve Length (L)	1.0	150.4	300.8	601.6	1203.1
	1.5	212.9	425.8	851.5	1703.1
	2.0	277.1	554.3	1108.5	2217.0
	2.5	342.2	684.4	1368.8	2737.5
Total Curvature (TK)	1.0	5.17	5.17	5.17	5.17
	1.5	8.29	8.29	8.29	8.29
	2.0	11.43	11.43	11.43	11.43
	2.5	14.57	14.57	14.57	14.57
Total squared curvature (TSK)	1.0	0.9536	0.4768	0.2384	0.1192
	1.5	3.2599	1.6300	0.8150	0.4075
	2.0	7.7571	3.8786	1.9393	0.9698
	2.5	15.1800	7.5898	3.7949	1.8975

To calculate the values of the geometric features and the tortuosity measures from the discrete parametrizations of the sinusoids, we computed the first and second derivatives $x_s'(k)$, $x_s''(k)$, $y_s'(k)$, $y_s''(k)$ and $x_i'(k)$, $x_i''(k)$, $y_i'(k)$, $y_i''(k)$. Direct calculation of these derivatives as differences between consecutive terms is unstable due to the noise affecting the parametrizations $C_s = (x_s(k), y_s(k))$ and $C_i = (x_i(k), y_i(k))$, even for an actual vessel segment extracted from a digital fundus image. While prior smoothing techniques are frequently suggested to address this issue, excessive smoothing can alter the curve's geometry. Instead, we followed the procedure described in our former work [5] and summarized here for the sake of clarity. We estimated the derivatives by a weighted least squares method [9] using the second order Taylor expansions of $x_s(k)$, $y_s(k)$, $x_i(k)$ and $y_i(k)$ at k_0 for a set of 10 points located on the curve at $k = \{k_0 \pm 1d, \dots, k_0 \pm Md\}$, with $M = 5$ to obtain an equivalent number of equations, in terms of the first and second derivatives at k_0. For the image size $A = 800$, d-value was set to $d = 4$. This choice ($d = 4$) is based on the width of some vessel segments found in digital fundus images with size 800×800. Vessel width can attain 7 pixels. Therefore, the points used extend up to 3 times the vessel width at either side of the point $(x(k_0), y(k_0))$, a length that we considered suitable to estimate curvature. For the scaled image versions, d-values were respectively set to 2, 1 and 1 for the A values 400, 200 and 100. The same procedure was used later for actual vessel segments extracted from real eye fundus images.

Based on the second order Taylor expansion of $x_s(k)$, the equations that allowed us to obtain estimations for $x_s'(k_0)$ and $x_s''(k_0)$ for any k_0 are:

$$x_s(k_0 + \beta d) \approx x_s(k_0) + x_s'(k_0) \cdot \beta d + \frac{1}{2} \cdot x_s''(k_0) \cdot (\beta d)^2, \qquad \beta = -5, \dots, 5 \tag{8}$$

The system was solved with weights equal to the inverse of the square root of the absolute value of the increments, i.e., $\frac{1}{\sqrt{|\beta d|}}$. Note that the points of the curve located close to its ends would have a reduced number of equations, M at least. The sequences $x'(k_0)$ and $x''(k_0)$ were finally smoothed using a 3-pixel moving average operator. We proceeded with $y_s(k)$, $x_i(k)$, and $y_i(k)$ in an analogous way. The resulting derivatives were used to calculate the curvature function (Eq. 1) for both C_s and C_i discrete parametrizations. Next, we calculated the geometric features and the tortuosity indices for all the sinusoids of Fig. 2. The results are contained in Table 6.

TABLE 6. Tortuosity values of the sinusoids (Fig. 2) for the continuous (C), discrete by sampling (C_s), and discrete from image (C_i) parametrizations.

Tortuosity index	parametrization	**Spatial frequency** $\omega = 1.0$ **Resolution** (A, pixels)				**Spatial frequency** $\omega = 1.5$ **Resolution** (A, pixels)			
		100	**200**	**400**	**800**	**100**	**200**	**400**	**800**
DF	C	2.50	2.50	2.50	2.50	3.54	3.54	3.54	3.54
	C_s	2.46	2.51	2.50	2.51	3.51	3.55	3.54	3.55
	C_i	2.26	2.43	2.48	2.50	3.41	3.50	3.52	3.54
T1	C	1.50	1.50	1.50	1.50	2.54	2.54	2.54	2.54
	C_s	1.46	1.51	1.50	1.51	2.51	2.54	2.54	2.55
	C_i	1.26	1.43	1.48	1.50	2.41	2.50	2.52	2.54
T2	C	5.17	5.17	5.17	5.17	8.29	8.29	8.29	8.29
	C_s	5.16	5.18	5.17	5.17	8.29	8.30	8.29	8.30
	C_i	5.14	5.17	5.17	5.17	8.28	8.30	8.29	8.30
T3	C	0.95	0.47	0.23	0.11	3.25	1.63	0.81	0.40
	C_s	0.9418	0.4790	0.2377	0.1193	3.2190	1.6360	0.8122	0.4077
	C_i	0.9418	0.4790	0.2377	0.1193	3.2190	1.6360	0.8122	0.4077
T4	C	0.034	0.017	0.008	0.004	0.038	0.019	0.009	0.004
	C_s	0.03545	0.01734	0.0086	0.00431	0.03931	0.01966	0.00976	0.00488
	C_i	0.03943	0.01829	0.00884	0.00436	0.04238	0.02040	0.00995	0.00493
T5	C	0.00634	0.00159	0.00040	0.00010	0.01531	0.00383	0.00096	0.00024
	C_s	0.00647	0.00161	0.00040	0.00010	0.01527	0.00388	0.00096	0.00024
	C_i	0.00723	0.00169	0.00041	0.00010	0.01648	0.00402	0.00097	0.00024
T6	C	0.08617	0.04308	0.02154	0.01077	0.13817	0.06908	0.03454	0.01727
	C_s	0.08729	0.04340	0.02153	0.01079	0.13810	0.06969	0.03456	0.01732
	C_i	0.08921	0.04449	0.02188	0.01089	0.14430	0.07148	0.03497	0.01743
T7	C	0.01589	0.00397	0.00099	0.00025	0.05433	0.01358	0.00340	0.00085
	C_s	0.01594	0.00402	0.00099	0.00025	0.05365	0.01374	0.00338	0.00085
	C_i	0.01635	0.00412	0.00101	0.00025	0.05615	0.01410	0.00343	0.00086
		Spatial frequency $\omega = 2.0$				**Spatial frequency** $\omega = 2.5$			
DF	C	4.61	4.61	4.61	4.61	5.70	5.70	5.70	5.70
	C_s	4.57	4.61	4.61	4.62	5.64	5.69	5.69	5.71
	C_i	4.33	4.49	4.58	4.60	5.62	5.66	5.66	5.70
T1	C	3.61	3.61	3.61	3.61	4.70	4.70	4.70	4.70
	C_s	3.57	3.61	3.61	3.62	4.64	4.69	4.69	4.71
	C_i	3.33	3.49	3.58	3.60	4.62	4.66	4.66	4.70
T2	C	11.43	11.43	11.43	11.43	14.57	14.57	14.57	14.57
	C_s	11.42	11.44	11.43	11.44	14.57	14.58	14.57	14.58
	C_i	11.42	11.44	11.43	11.44	15.56	14.58	14.57	14.58
T3	C	7.75	3.87	1.93	0.96	15.18	7.58	3.79	1.89
	C_s	7.6630	3.8950	1.9340	0.9705	15.00	7.6230	3.7840	1.8990

	C_i	7.6630	3.8950	1.9340	0.9705	15.00	7.6230	3.7840	1.8990
T4	C	0.041	0.020	0.010	0.005	0.042	0.021	0.010	0.005
	C_s	0.04165	0.02081	0.01034	0.00517	0.04301	0.02148	0.01067	0.00532
	C_i	0.04409	0.02141	0.01048	0.00521	0.04507	0.02198	0.01069	0.00535
T5	C	0.02799	0.00700	0.00175	0.00044	0.04436	0.01109	0.00277	0.00069
	C_s	0.02794	0.00709	0.00175	0.00044	0.04428	0.01123	0.00277	0.00069
	C_i	0.02960	0.00729	0.00177	0.00044	0.04642	0.01150	0.00280	0.00070
T6	C	0.19050	0.09525	0.04763	0.02381	0.24283	0.12142	0.06071	0.03035
	C_s	0.19040	0.09595	0.04763	0.02387	0.24280	0.12220	0.06072	0.03036
	C_i	0.19110	0.09616	0.04797	0.02395	0.24890	0.12430	0.06115	0.03048
T7	C	0.12929	0.03232	0.00808	0.00202	0.25300	0.06325	0.01581	0.00395
	C_s	0.12770	0.03268	0.00806	0.00203	0.24990	0.06388	0.01576	0.00396
	C_i	0.12830	0.03276	0.00811	0.00203	0.25630	0.06501	0.01588	0.00397

Continuous $C = (x(t), y(t))$ (Eq. 6)
Discrete by sampling $C_S = \left(x_s(t), y_s(t)\right)$ (Eq. 7)
Discrete from image plot $C_i = \left(x_i(t), y_i(t)\right)$

All tortuosity indices increase with increasing frequency, but not with similar behavior. $T4$ increases very slowly with frequency.

The tortuosity values obtained from both C_s and C_i discrete parametrizations are similar to the corresponding tortuosity measures obtained from the continuous parametrization C in general for all the indices. Small discrepancies between those C, C_s and C_i parametrizations can be found, however, for the images with the lowest resolution ($A = 100$). This is likely due to a poorer graphical description of the sinusoids, which may affect more severely the parametrization obtained from the sinusoid plot image (C_i). As expected from Table 4, DF, $T1$, and $T2$ result unaffected or barely affected by scaling (change of the image size A) across all frequencies and parametrizations. However, the remaining indices $T3 \ldots T7$ exhibit strong sensitivity to scaling. For a given frequency, these indices decrease as image size A increases, in accordance with the scale factors specified in Table 4. It is noteworthy that these indices can be even more sensitive to scaling than to a change in frequency, potentially leading to misinterpretations when comparing tortuosity values across images of varying resolutions.
For instance, the $T3$ values measured for frequency $\omega = 2.5$ in the 800×800 image are not greater than the $T3$ values measured for the lower frequency $\omega = 2$ in the 400×400 image, even though they should be higher. Similar discrepancies are observed for $T5, T6,$ and $T7$ values measured for frequency $\omega = 2.5$ in the 800×800 image, which result to be lower than the respective tortuosity values measured for lower frequencies in quite a few lower-resolution images. In particular, $T4$ exhibits the most pronounced sensitivity to scaling. The $T4$ values measured across all three parametrizations for the highest frequency of $\omega = 2.5$ in the 800×800 image are lower than all $T4$ values obtained in lower-resolution images ($A = 100, 200, 400$) for any lower frequency $\omega = (1, 1.5, 2)$.

4. Resolution effects for an actual retinal vessel segment

This study can also be extended to the centerline of a vessel segment extracted from a digital fundus image. In the example illustrated in Fig. 3 a vessel segment is painted in cyan in the original 800×800 eye fundus image and three scaled versions. In our previous work [5] we described the method followed to obtain vessel centerlines. By means of a MATLAB interface, the user can roughly trace an approximate path along the vessel segment of interest in a fundus retinal image. Following the method described in [5], the vessel tree is subsequently segmented from a region wide enough around the traced path. Endpoints and bifurcation points are identified from the skeletonization of the segmented vessel tree. Nonessential branches are excluded. As a result, we obtain an approximation of the centerline for the selected vessel segment.

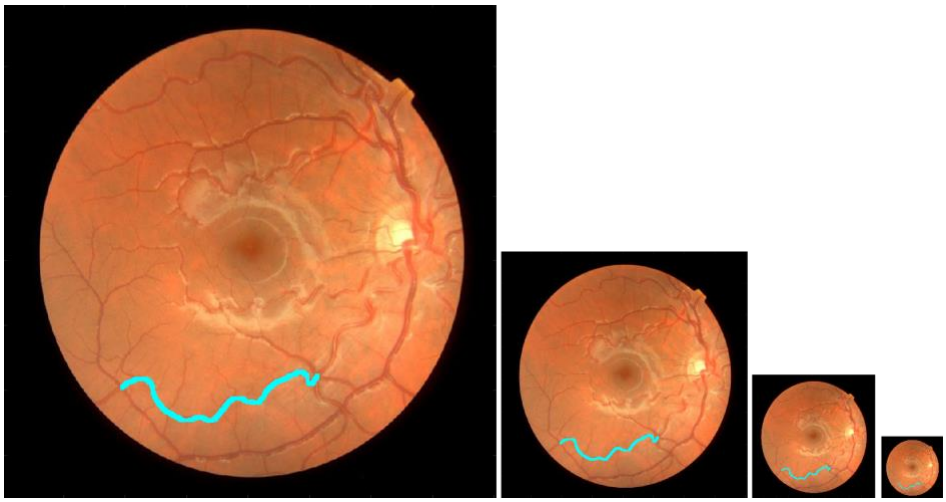

Fig 3. Vessel segment (in cyan) marked in the original 800 × 800 eye fundus image and scaled versions.

Table 7 summarizes the tortuosity measures (in black) corresponding to the vessel segment shown in Fig. 3 and its scaled versions. These values were obtained from the C_i parametrization of the curve plot in the original and resized images. Below every value in black, another value (in red) provides an estimate from the value found for the 800 × 800 image scaled by the corresponding factor specified in Table 4. Observe that the actual tortuosity value (black) is lower than this estimation (red) across all the indices and resized versions ($A = 100, 200, 400$). The percentage amount (%) needed to attain the estimated value is given in brackets. We can hypothesize that these estimated values would be reached if only the scale effect was involved with no further loss of information. The comparison of both, the actual and the estimated values for each tortuosity index, reveals the impact of the resolution change.

TABLE 7. Tortuosity measures for the vessel segment of Fig. 3 in the original image and scaled versions. In black, actual value computed using the C_i parametrization; in red, estimated value calculated by applying the scaling effect predicted in Table 4 on the actual value obtained for the original 800 × 800 image. The discrepancy between these two values, the estimated and the actual, is presented by a ratio in percentage (in brackets).

Tortuosity index	Resolution (A, pixels)			
	100	200	400	800
DF	1.2288 1.2605 (2.6%)	1.2311 1.2605 (2.4%)	1.2520 1.2605 (0.7%)	1.2605
T1	0.2288 0.2605 (13.9%)	0.2311 0.2605 (12.7%)	0.2520 0.2605 (3.4%)	0.2605
T2	8.1448 9.4580 (16.1%)	8.2657 9.4580 (14.4%)	9.0007 9.4580 (5.1%)	9.4580
$T3$	2.3858 3.0736 (28.8%)	1.1788 1.5368 (30.4%)	0.6959 0.7684 (10.4%)	0.3842
$T4$	0.1699 0.1944 (14.4%)	0.0872 0.0972 (11.5%)	0.0467 0.0486 (4.1%)	0.0243
$T5$	0.0498 0.0640 (28.5%)	0.0124 0.0160 (29.0%)	0.0036 0.0040 (11.1%)	0.0010
$T6$	0.2088 0.2448 (17.2%)	0.1073 0.1224 (14.1%)	0.0584 0.0612 (4.8%)	0.0306
$T7$	0.0612 0.0768 (25.5%)	0.0153 0.0192 (25.5%)	0.0045 0.0048 (6.7%)	0.0012

As anticipated from Table 4, the DF, $T1$, and $T2$ indices exhibit remarkable stability across varying image resolutions, with DF being the most consistent by far. However, slight discrepancies can be identified between the actual and estimated values of these indices for low-resolution images. These low-resolution images typically provide an incomplete representation of the vessel's intricate path, leading to slightly lower tortuosity estimations. For the rest of indices $T3 \ldots T7$, the tortuosity values (grey-shaded cells in Table 7) are clearly susceptible to scale changes, as predicted in Table 4. The discrepancies between the estimated and actual values for low-resolution image versions (percentages are provided in brackets in

Table 7) are generally much higher than those for the DF index. Notably, indices based on the total squared curvature ($T3, T5$, and $T7$) exhibit stronger susceptibility to information loss due to resolution changes, with discrepancies reaching approximately 30% for certain low-resolution versions.

5. Discussion and conclusions

The impact of scaling and subsequent resolution changes in eye fundus images has been examined for a set of tortuosity indices $\{DF, T1 \ldots T7\}$ and both simulated and actual retinal vessel segments. To better address this issue, we utilized sinusoids of varying frequencies to simulate vessel segments of diverse tortuosity and considered three parametrizations: continuous (C), discrete based on sampling (C_s), and discrete based on the image (C_i). We employed square images with dimensions 800, 400, 200, and 100 pixels.

As Tourior et al. [7] emphasized, a tortuosity index should be independent of scale, implying that a magnified or reduced image of a particular vessel shape should exhibit nearly identical tortuosity values compared to the original image. This property is theoretically preserved solely for DF, $T1$ and $T2$ (Table 4). In practice, the results obtained with these indices are in excellent alignment with theoretical expectations. In particular, DF, the simplest and most widely used index, has demonstrated superior performance in terms of the important criterion of scale-independence.

The remaining indices ($T3, \ldots, T7$) do not exhibit scale-independence (Table 4). The tortuosity values obtained with the $T3, T4$, and $T6$ indices are inversely proportional to the scale factor, while those obtained with the $T5$ and $T7$ indices are inversely proportional to the square of the scale factor. The pronounced dependence of $T3, \ldots, T7$ on scale makes this criterion particularly significant when comparing tortuosity values measured in original images of different resolution. It is crucial to adequately compensate for the image resolution difference prior to comparing these values. Otherwise, the variation of these indices with the vessel tortuosity could be masked by the scale difference between the original images.

In addition to the expected effects solely attributable to scaling, we observed fluctuations with all indices, potentially due to the loss of geometric features in the low-resolution versions. Most detrimental discrepancies were encountered for the indices based on the total squared curvature ($T3, T5, T7$) and resolutions lower than 400×400 (with the estimated to actual tortuosity value ratio approaching 30%).

The tortuosity indices that satisfy the scale-independence criterion may not necessarily be the most suitable for other criteria. For instance, with regard to the frame centering of a digital fundus image (either at the optic disc or at the macula), we found that the $T4$ index exhibited the highest robustness against frame center changes (macula to disc) among the eight indices $\{DF, T1 \ldots T7\}$ analyzed [5]. However, $T4$ would not be the most appropriate choice when considering the scale-independence criterion.

The effect of the parametrization on the value of the tortuosity indices is nearly negligible for all studied frequencies and resolutions of the simulated vessels (sinusoids), with more pronounced discrepancies in the low-resolution versions. Therefore, suitable resolutions should be employed to minimize this effect.
The findings of this study provide valuable insights for comparing tortuosity values measured in different images and resolution conditions. However, our study is not without limitations. We analyzed images with resolutions up to 800×800 pixels and simulated sinusoidal vessels with limited range of frequency. Rotation effects in the simulated or segmented curves were not considered.

7. Acknowledgements

The authors acknowledge Dr. Laura Clavé, optometrist, for her dedicated collaboration in retinal image acquisition and the Hospital de Mataró (Consorci Sanitari del Maresme, Barcelona, Spain) for providing us with the anonymized eye fundus images. This research was funded by the Ministerio de Ciencia e Innovación, Agencia Estatal de Investigación (AEI) of the Spanish Government. Project reference number PID2020-114582RB-I00/AEI/10.13039/501100011033.

